Composites: Part A 41 (2010) 1461–1470

Contents lists available at ScienceDirect

Composites: Part A

journal homepage: www.elsevier.com/locate/compositesa

Artificial lightning testing on graphite/epoxy composite laminate

Yoshiyasu Hirano [a,*], Shingo Katsumata [b], Yutaka Iwahori [a], Akira Todoroki [c]

[a] Japan Aerospace Exploration Agency (JAXA), Advanced Composite Group, Aerospace Research and Development Directorate, 6-13-1, Ohsawa, Mitaka-shi, Tokyo 181-0015, Japan
[b] Graduate School of Tokyo Institute of Technology, 2-12-1-I1-58 Ookayama, Meguro-ku, Tokyo 152-8552, Japan
[c] Tokyo Institute of Technology, Department of Mechanical Sciences and Engineering, 2-12-1-I1-58 Ookayama, Meguro-ku, Tokyo 152-8552, Japan

ARTICLE INFO

Article history:
Received 26 March 2009
Received in revised form 28 April 2010
Accepted 19 June 2010

Keywords:
A. Laminates
B. Fracture
C. Damage mechanics
D. Non-destructive testing

ABSTRACT

This study examines the evolution of damage in graphite/epoxy composite laminates due to lightning strikes. To clarify the influence of lightning parameters and specimen size, artificial lightning testing was performed on a series of laminated composite specimens. Damage was assessed using visual inspection, ultrasonic testing, micro X-ray inspection, and sectional observation. The results showed that the damage modes can be categorized into fiber damage, resin deterioration, and internal delamination modes. Damage progression is governed by the strong electrical orthotropic properties of the laminates, and the lightning parameters defining impulse waveform show strong relationship with certain damage modes, though specimen size and thickness variation barely affect damage size.

1. Introduction

At present, because of their potential for reducing weight, graphite/epoxy laminated composites are being planned for widespread use in principal structures of new-generation commercial aircraft. Although these advanced composites have superior mechanical properties compared to conventional aluminum alloy, they usually show large strength degradation because of internal damage such as delamination and matrix cracks. One of the major causes of internal damage is impact through tool dropping and fragment hits during manufacturing, maintenance, or operation. Lightning strikes are another possible cause of internal damage to laminated composite structure [1].

Internal damage due to impact has been investigated by a number of researchers, and detailed damage mechanisms have been clarified [2–5]. The direct effect of lightning strikes on laminated composite structures and their damage behavior have also been investigated [6,7], and on the basis of the investigation results, lightning protection systems for direct and indirect effects have been proposed [8]. However, it is difficult to prevent damage completely even if the appropriate lightning protection systems are applied to the composite structure. Therefore, damage to a composite as a direct effect of a lightning strike during a flight may be a major issue in terms of aircraft durability and long-term operation [9]. In some regions in particular, such as the coast of the Japan Sea and the west coast of Norway, the occurrence of winter lightning having large amounts of energy with long-term discharge along with loud and long thunderclaps has been reported [10]. Although clarifying the effects of unusual lightning strikes is important, the effect of the energy or waveform variation of lightning strikes on damage to composite structures has attracted little attention. In addition, detailed mechanisms of fractures due to direct effect of lightning strikes on composite structures have yet to be clarified.

In this study, therefore, in order to investigate the basic damage mechanisms of graphite/epoxy laminated composite due to lightning strikes, focusing on the relationship between variations in lightning strike waveform and damage dimensions, an artificial lightning test that simulates a natural lightning stroke was performed on graphite/epoxy laminated composite specimens with no lightning protection system. The damage mode and dimensions were investigated by visual inspection and several forms of non-destructive testing.

2. Experimental methods

2.1. Specimens

The material used in this study was a graphite/epoxy laminate made of toughened epoxy resin #133 and medium-modulus/high-strength IM600 graphite fiber produced by Toho Tenax. IM600/133 has been developed for aerospace usage and has high compression-after-impact (CAI) strength. The composite was processed by prepreg molding in an autoclave following a recommended cure cycle. For the artificial lightning test, laminates with four types of stacking sequence were prepared: [45/0/−45/

* Corresponding author. Tel.: +81 42240 3564; fax: +81 42240 1451.
E-mail address: hirano.yoshiyasu@jaxa.jp (Y. Hirano).

1359-835X/$ - see front matter © 2010 Elsevier Ltd. All rights reserved.
doi:10.1016/j.compositesa.2010.06.008

$90]_2$s, $[45/0/-45/90]_3$s, $[45/0/-45/90]_4$s, and $[45/0/-45/90]_5$s. The thicknesses of the laminates were $t = 2.3$, 3.5, 4.7, and 5.8 mm, respectively. The sizes of the specimens were selected with reference to ASTM D7137 [11]: the residual strength test standard for polymer matrix composites. The specimens were cut out from the parent laminates in dimensions of 350 mm × 350 mm.

2.2. Experimental setup

In order to simulate lightning strikes, an impulse high-voltage generator (IVG) produced by Haefely test AG (see Fig. 1) and an impulse high-current generator (ICG) produced by Nisshin Electric Co. (Fig. 2) were used in this study. The IVG can generate an impulse current with high maximum current but only for a short time. On the other hand, the ICG can generate a long-term impulse current but with low maximum current amplitude. The IVG is equipment for generating high voltage impulse in nature. However, in this study, the wiring pattern of capacitance was modified to generating high-current impulse as with ICG. Therefore, the most suitable generator was selected according to each test condition. Fig. 3 schematically shows the cursory circuit of the generators, where Rs and Ro are resistances and Cs is capacitance. By varying Rs, Ro, and Cs, an arbitrary waveform can be generated. Here, for the ICG, Ro is always set as zero. A DC current transformer (DCCT) was connected to the ground wire from the specimen, and the waveform of the applied impulse current was measured using an oscilloscope. A detailed description of the lightning test equipment and setup used can be found in [12].

The specimens were placed on a test jig, which mainly comprises two 15-mm-thick glass fiber/epoxy (GFRP) laminates and a discharge probe made from SUS304. The lower GFRP laminate supported the specimen and the upper laminate held the probe. The upper GFRP laminate was supported by four GFRP threaded rods so that the distance between the laminates can be adjusted with screws. The distance between the tip of the discharge probe and specimen surface was adjusted to about 2.0–3.0 mm. To ensure an earth ground connection with the specimens, a copper sheet connected to the earth ground was inserted between the specimens and the lower GFRP laminate. A schematic of the testing setup and the dimension of the discharge prove is shown in Fig. 4a and b, respectively.

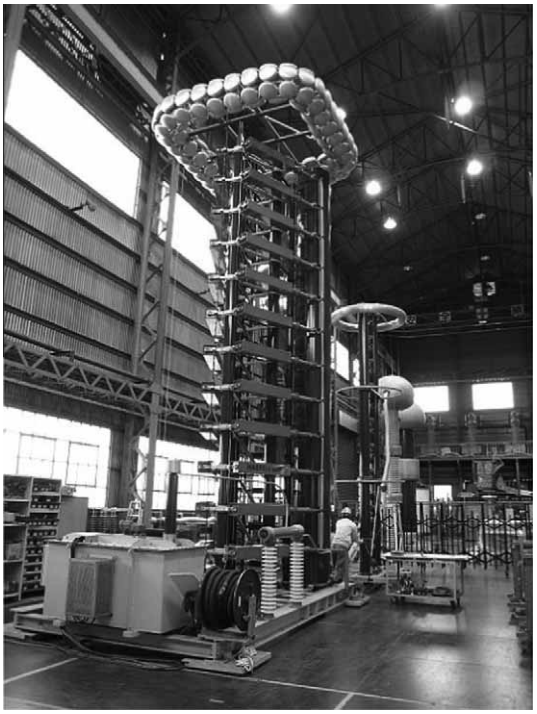

Fig. 1. Modified impulse voltage generator (IVG) produced by Haefely test AG.

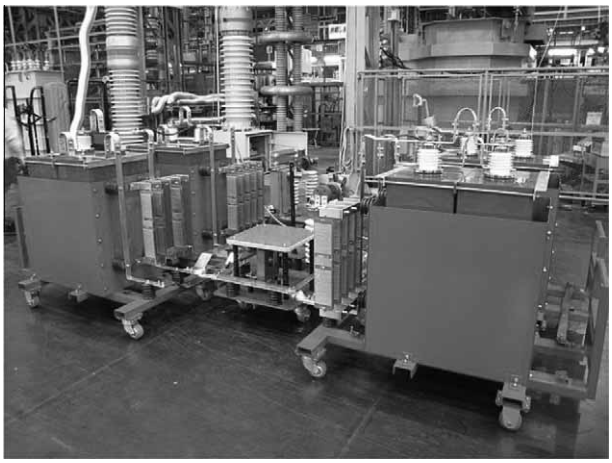

Fig. 2. Impulse current generator (ICG): produced by Nisshin Electric Co.

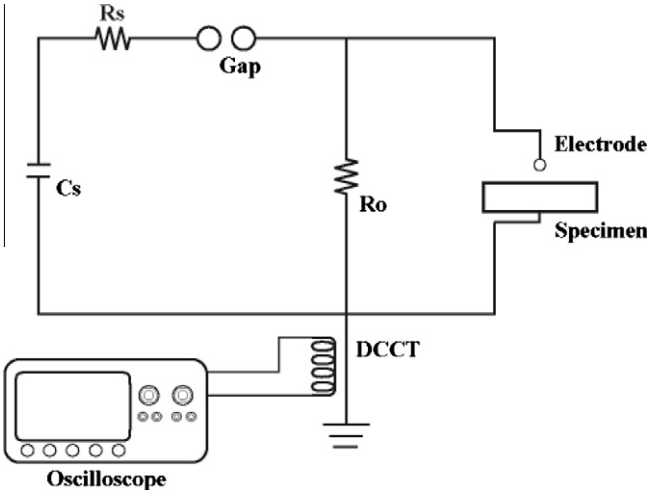

Fig. 3. Illustration of circuit for the impulse testing machine.

2.3. Testing condition and artificial lightning waveform

The tested impulse waveform conditions are listed in Table 1. Systematic experimental conditions were examined so that when a graphite/epoxy composite laminate comes into contact with an impulse current waveform, the responses can be understood and characterized. Usually, natural lightning displays complicated time series variation in current waveform. For simplification, the lightning environment has been synthesized from negative and positive natural lightning characteristics into components designated A–D. A natural lightning environment and descriptions of the standard lightning environment for aircraft design are described in a committee report by the SAE [13].

In this study, for component A of a positive first return stroke, three types of waveforms with differing duration times were tested as listed in Table 1. The impulse waveforms are defined with a pair of numbers: the first number represents the time to peak and the latter represents the time to half the value (see Fig. 5). For example, for T_1/T_2 [μs], the time from 10% to 90% of the maximum current is T_1 [μs], and the time from 10% to 50% through 90% of the maximum

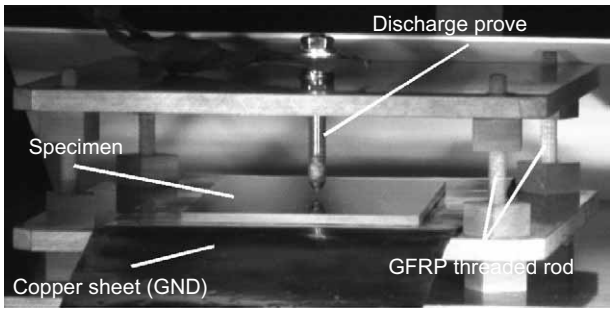

(a) Support jig and specimen setup

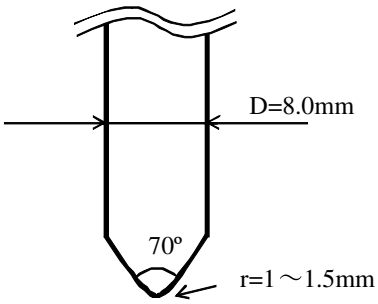

(b) schematic of discharge plove and dimensions

Fig. 4. Experimental setup.

current is T_2 [μs]. Electrical charge (Q) and action integral (AI) shown in Table 1 represent the total energy and specific energy of the impulse current, respectively, as follows:

$$Q = \int i\mathrm{d}t \tag{1}$$

$$I = \int i^2\mathrm{d}t \tag{2}$$

where i is the time-varying electrical current of lightning waveforms.

3. Results and discussion

3.1. External damage due to lightning strike

According to the test conditions listed in Table 1, artificial lightning tests were performed on 40 specimens. Conditions I–VI were tested using the IVG (Fig. 1), and conditions VII and VIII were tested using the ICG (Fig. 2). The typical measured electrical current

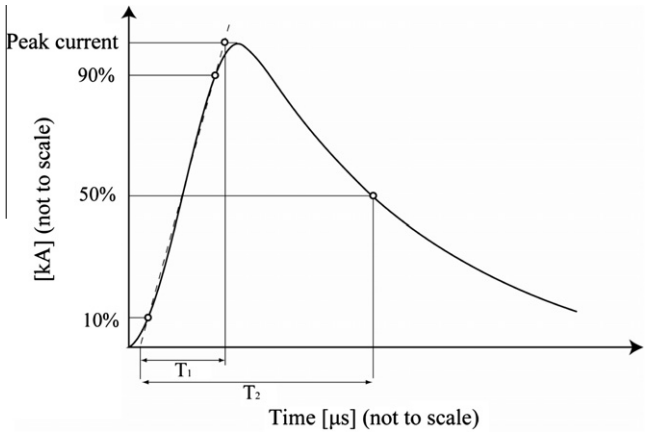

Fig. 5. Impulse waveform definition.

waveform with the modified IVG (condition IV) and the ICG (condition VII) is shown in Fig. 6a and b, respectively. As shown in the figure, both testing equipment can be generate the desired waveform, though the modified IGV result shows the oscillated reaction in its later damping phase.

The visual appearance of the tested specimen is shown in Fig. 7a–h. Each figure represents overhead view of the typical result of the specific test condition. Here, the test result with condition IV (4/20 μs with peak current of 40.0 kA) is shown in Fig. 8 as a typical result of an artificial lightning test. Fig. 8a shows the overhead view, and Fig. 8b shows a magnified view of lightning strike attachment point. Through visual inspection, two typical damage modes can be observed. At the lightning attachment point, carbon fiber breakage can be observed several layers deep from the lightning attachment surface; fiber dissipation and resin vaporization can also be observed in a region roughly 20 mm in diameter. (This damaged region is referred to hereafter as fiber damaged area.) At the same time, a strip-shaped ply-lift in the fiber direction of the outermost 45° layer is observed. The ply-lift initiation point is the lightning attachment point, and the width is almost the same as the diameter of the fiber damaged area. Outside the surface fiber damage region, resin deteriorated area where has fuliginous and blistered surface can be observed (see Fig. 8b). In this study, this region of deterioration is referred to as the resin deterioration area. Since the resin deterioration area has the different reflectance from the intact surface, damaged region can be determined by means of an image processing. First, overhead view of post-lightning specimen is converted into grayscale image data. Then, the image is binarized using histogram information of the image data. A typical image binarization result is shown in Fig. 8c as an example. Here, the pretreatment image is Fig. 8a. The black region represents the resin deterioration area obtained by image processing.

Table 1
Testing conditions for artificial lightning test.

	Waveform	Peak current (kA)	Electrical charge (C)	Action integral (A^2 s)	Stacking sequence	Number of tests
I		40.0	0.49	11,500		3
II	2.6/10.5	30.0	0.37	6300	$[+45/0/-45/90]_{4S}$	4
III		20.0	0.2	2900		3
					$[+45/0/-45/90]_{2S}$	2
IV	4/20	40.0	0.85	22,000	$[+45/0/-45/90]_{3S}$	2
					$[+45/0/-45/90]_{4S}$	5
					$[+45/0/-45/90]_{5S}$	2
V		30.0	0.63	12,000	$[+45/0/-45/90]_{4S}$	5
VI		20.0	0.42	5500		5
VII	7/150	20.0	3.71	40,000	$[+45/0/-45/90]_{4S}$	6
VIII		10.0	1.61	3500		3

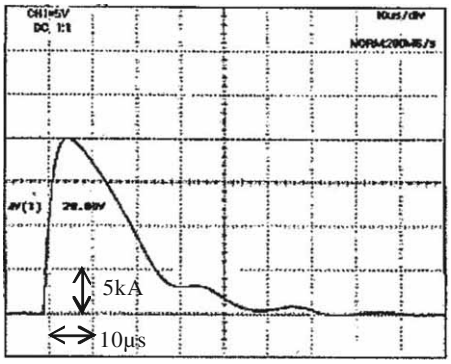

(a) tested waveform with modified IGV (condition IV)

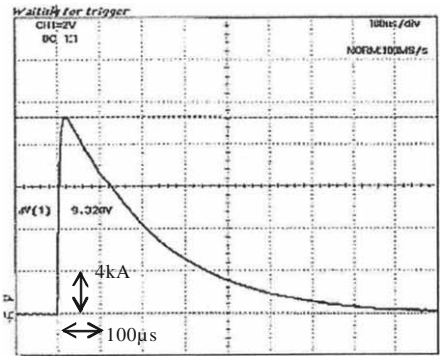

(b) tested waveform with ICG (condition VII)

Fig. 6. Measurement results of applied waveform.

On the other, any damage could not be observed on the specimen surface opposite from the lightning attachment side. After the discharge test, signature of the spark discharge could be observed on the surface of the copper plate along the specimen's edge. This indicate that the applied electrical current flown the in-plane direction inside of specimen from the impulse attached point of the specimen surface to specimen edge across the inside of specimen. Then the current spark between the specimen edge and copper plate; and electrical current finally flow into the earth ground.

One of the major causes of fiber damage is considered to be shockwaves due to supersonic-speed expansion of the ionized leader channel when a return stroke occurs [8]. However, focusing on the lightning attachment point, it can be observed that most of the resin was burned off or evaporated by the heat. Since carbon fiber has a relatively high electrical conductivity, a resistive heating effect cannot be neglected. As temperature rises through resistive heating, the burning or pyrolysis of resin advances, and reacted resins release gas. The rapid evaporation of trapped gas in interlaminar layers results in an explosive fracture in the vicinity of the lightning stroke attachment point. Therefore, the combination of a shockwave event and a rapid evaporation of resin through resistive heating is a major cause of explosive fractures of surface fiber.

Similarly, it is considered that the cause of resin deterioration is the combined effect of the resistive heating of the surface layer and high atmospheric temperature due to insulation breakdown of air. The high atmospheric temperature induced by the delivery of a large amount of energy to the leader channel causes resin evaporation and deterioration in the same way as for resistive heating. It has previously been reported that atmospheric temperature

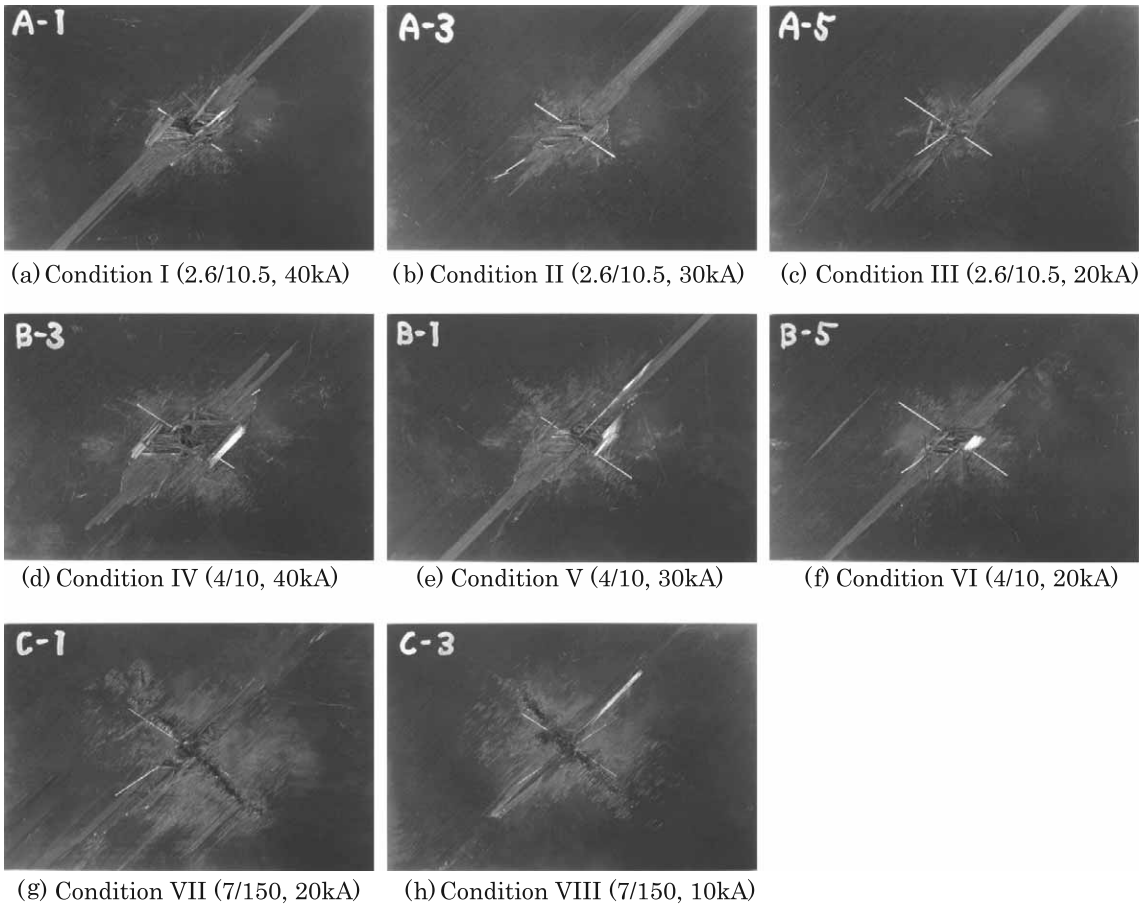

(a) Condition I (2.6/10.5, 40kA) (b) Condition II (2.6/10.5, 30kA) (c) Condition III (2.6/10.5, 20kA)

(d) Condition IV (4/10, 40kA) (e) Condition V (4/10, 30kA) (f) Condition VI (4/10, 20kA)

(g) Condition VII (7/150, 20kA) (h) Condition VIII (7/150, 10kA)

Fig. 7. Overhead view of post-lightning specimen.

(a) Overhead view of damaged specimen

(b) Magnified view of lightning attachment point

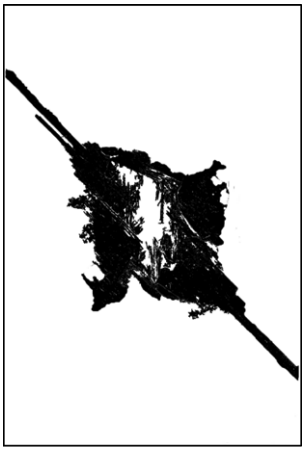

(c) Resin deterioration area obtained by image binarization

Fig. 8. Specimen after artificial lightning strike (condition IV: 4/20 μs, 40 kA, t = 4.7 mm).

around the ionized leader channel of a natural lightning strike reaches up to 30,000 K [8]; the starting temperature of pyrolysis for common epoxy resin is around 600 K, which is considerably lower than the heated atmospheric temperature due to lightning strikes.

3.2. Internal damage

In order to examine the internal damage, a non-destructive inspection (NDI) was performed using ultrasonic testing (UT). The UT inspection system consists of a three-axis computer-controlled scanning bridge, a high frequency ultrasonic parser/receiver (produced by Krautkramer Japan, Co. LTD), and echo signal acquisition system G-SCAN 3AX 300SR (produced by GNES Co.).

The UT test results for post-lightning test are shown in Fig. 9a–h. Each figure represents C-scan image of the typical result of the specific test condition. UT scanning results were obtained from the opposite side of the lightning attachment surface with a 5.0 MHz transducer. Fig. 10 represents the C-scan image for test condition of IV (20/40 μs, 40 kA, t = 4.7 mm), as in the previous section. The results show that the lightning tests created large delaminations; the delamination propagates in the shape of a pair of fans along the fiber direction starting from the lightning attachment point in each interlayer. Focusing on the B-scope result, it can be observed that the internal damage area is limited to the vicinity of the damaged surface in the direction of thickness. However, it is considered that the delamination is clearly distinguished from resin deterioration area described in the previous section; they can be distinguished as different damage mode. For purpose of comparison, the overlaid image of UT scanning and the resins deterioration area is shown in Fig. 11; the outline of the delamination obtained from the UT scanning image (Fig. 10) is shown as overlaid image with the binarized image for resin deterioration area (Fig. 8c). Since the resin deterioration area is obviously smaller than the delamination area, this indicates the cause of the damage propagation is different between resin deterioration and delamination.

For comparison, the UT scan result for typical internal damage caused by drop weight impact is shown in Fig. 12. The drop weight test was performed in reference to ASTM D7136 [14] on an identical specimen used in the lightning tests; detailed descriptions of the drop weight test can be found in the test standard. Comparing this with the result of the lightning test, it can be clearly seen that both damage propagations in the in-plane direction are quite similar: delamination in both the lightning test and the drop weight test propagate in the shape of a pair of fans in each interlayer. However, looking at the direction of thickness, though the internal damage area due to lightning strikes is limited to the vicinity of damaged surface as previously described, the internal damage due to impact propagates across the entire thickness of the specimen.

For detailed investigation of internal damage in the direction of thickness, a cross section of the specimen was observed with a digital microscope VHX-500 produced by Keyence Co. Figs. 13 and 14 show a series of sectional observation results, illustrating the relationship between the sectional observation results and the location of cutout lines in the specimen. The distance between the adjacent cutout lines is 3 mm.

The results show that damage due to lightning occurs in more than a dozen layers from the surface of the lightning attachment, as observed in the UT B-scope result. Furthermore, the damage is composed of delaminations and matrix cracks; several delaminations occurring in different interlayers are connected by matrix cracks propagating in the direction of thickness. This series of results indicate that internal damage has a sterical distribution inside the laminate. For example, focusing on the largest delamination, the middle point of the delamination is located at the center of the specimen just beneath the lightning attachment point (see Fig. 13b). It is observed that the middle point gradually shifts in the longitudinal direction (y) with an increase in the distance between the cutout line and the lightning attachment point (from cross section B to D). This indicates that delamination progresses in the fiber direction in each layer. Since the fiber direction is different in each layer, total internal damage due to lightning strikes must have a sterical configuration.

To understand damage propagation behavior due to lightning strikes, the electrical properties of graphite/epoxy laminates used in this study were measured with an LCR meter. For measurement,

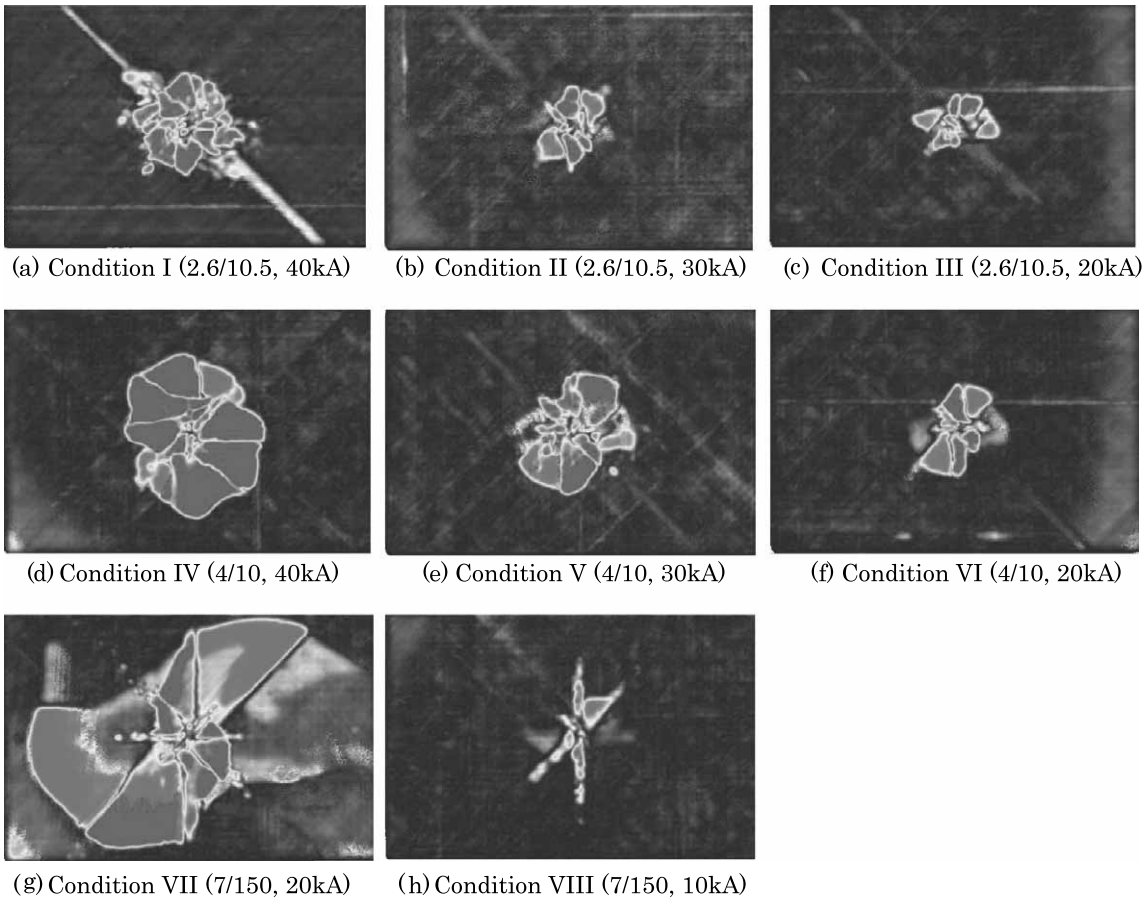

Fig. 9. C-scan image of post-lightning specimen.

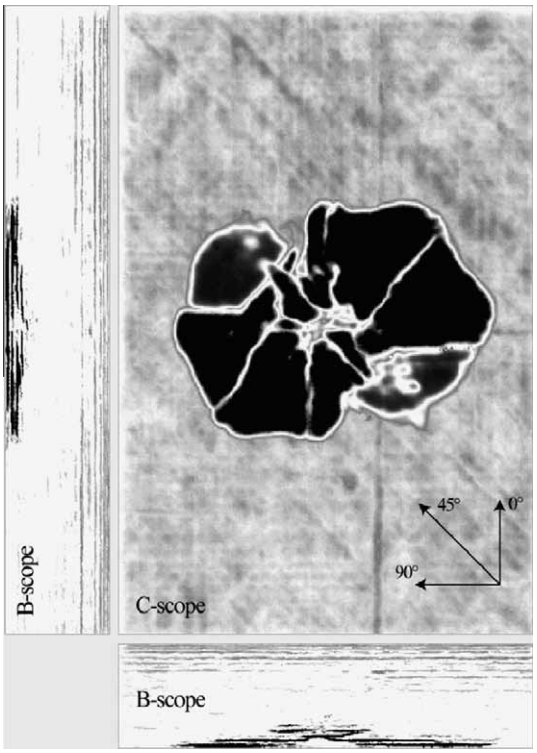

Fig. 10. Ultrasonic testing result of artificial lightning test.

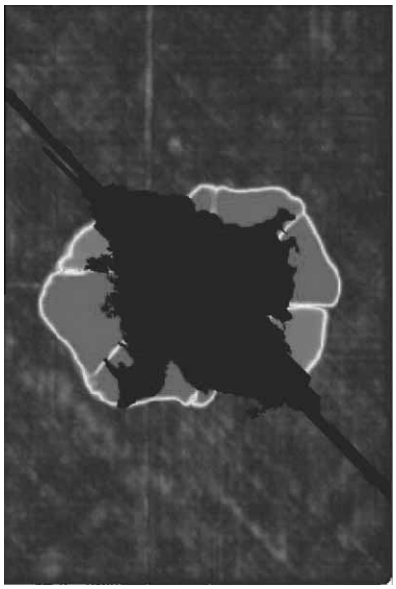

Fig. 11. The overlaid image of UT scanning and the resins deterioration area.

copper electrodes were electroplated on the surface of the specimens. The measurement method is described in more detail in [15,16]. The results are shown in Table 2. For comparison, the specific resistance of HTA7/CIBA913 measured by Abry et al. [16] is

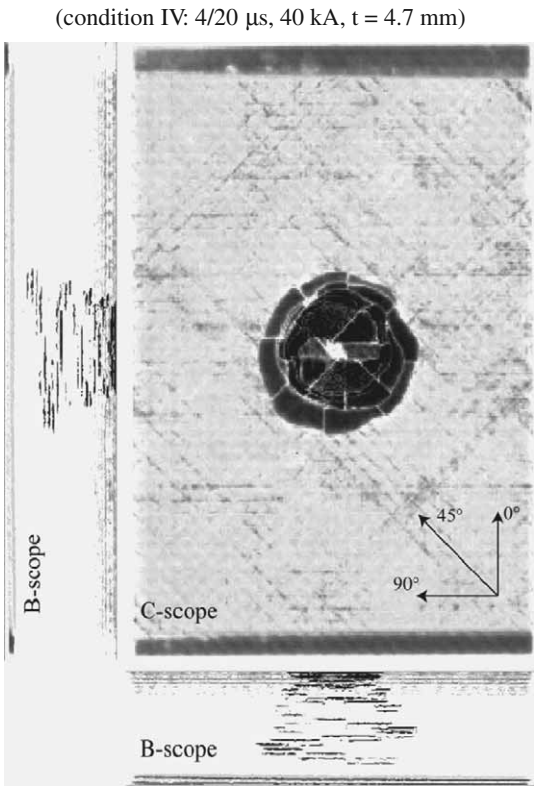

Fig. 12. Ultrasonic testing result of drop weight impact test (6.7 J/mm).

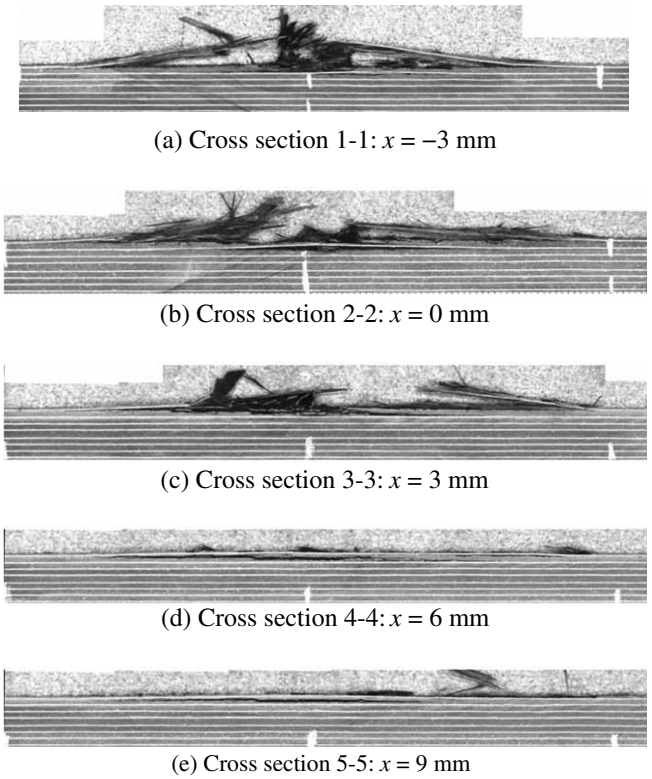

Fig. 13. Sectional observation results (condition IV: 4/20 μs, 40 kA, t = 4.7 mm).

also shown in Table 2 as typical electrical properties of unidirectional graphite/epoxy laminate. The results show that CFRP has anisotropic electrical properties in the transverse and thickness

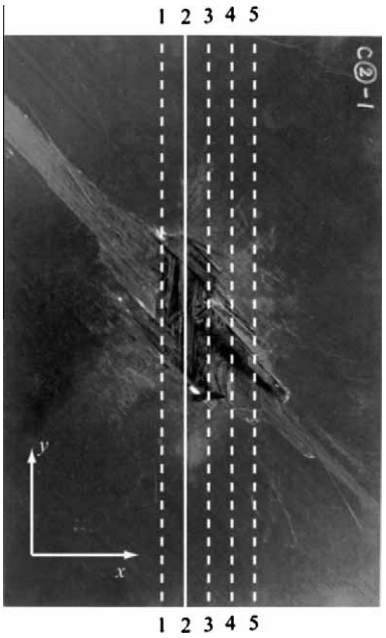

Fig. 14. Indication of cutout line and definition of coordinates.

directions, and the specific resistance of CFRP laminates depend strongly on its fiber volume fraction. However, the specific resistance in the transverse and thickness directions of IM600/133 (V_f = 60.2%) is determined to be larger than that of HTA7/CIBA913 (V_f = 43.0%). This is because an aerospace grade CFRP, IM600/133, has a relatively thicker resin interlayer so as to improve impact damage resistivity. This resin-rich layer acts as an insulator and increases the specific resistance of IM600/133 in the transverse and thickness directions.

It is considered that this strong orthotropic electrical conductivity in the longitudinal/transverse direction induces the delamination propagating in the shape of a pair of fans in each interlayer as observed in the UT C-scan image (see Fig. 10). On the other, the orthotropic electrical property of the longitudinal/thickness direction limits damage propagation in the thickness direction for more than a dozen layers from the specimen surface.

3.3. Specimen size variation effect on damage size

Several thickness specimens were examined under a specific test condition (condition IV, 4/20 μs, 40 kA) for understanding the effect of specimen thickness on damage behavior. The tested specimens were quasi-isotropic laminates of [45/0/−45/90]ns, n = 2–5 stacking sequence, with thicknesses of t = 2.3, 3.5, 4.7, and 5.8 mm, respectively. Fig. 15 represents the results of measured maximum damage depth obtained using a micro X-ray CT scanner (Toscaner-30000mhd, Toshiba Co.) following a lightning test. All the measured results of the maximum damage depth are virtually the same despite the variation in thicknesses of the target specimens. Fig. 16 represents the measured results of fiber damaged area, resin deterioration area, and delamination area. The fiber damaged area and resin deterioration area were determined by measuring the damaged area from an overhead view image of the tested specimens. The delamination area was determined using a C-scan image of UT as a projection area. The results are shown as averaged values obtained from two tests. The results show that there are no significant differences for each damage mode despite the target specimens varying in thickness. As described in the previous section, a lightning damage region in the thickness direction is limited to the vicinity of the

Table 2
Electrical properties of uni-directional CFRP laminate.

	V_f (%)	Longitudinal resistivity ρ_L (Ω m)	Transverse resistivity ρ_{tw} (Ω m)	Thickness direction resistivity ρ_{tt} (Ω m)
IM600/133	60	2.78×10^{-5}	8.73×10^{-1}	5.58×10^{2}
HTA7/CIBA913	43	4.72×10^{-5}	4.67×10^{-1}	1.6×10^{1}
	49	3.71×10^{-5}	1.13×10^{-1}	2.83
	58	2.93×10^{-5}	4.16×10^{-1}	4.82×10^{-2}

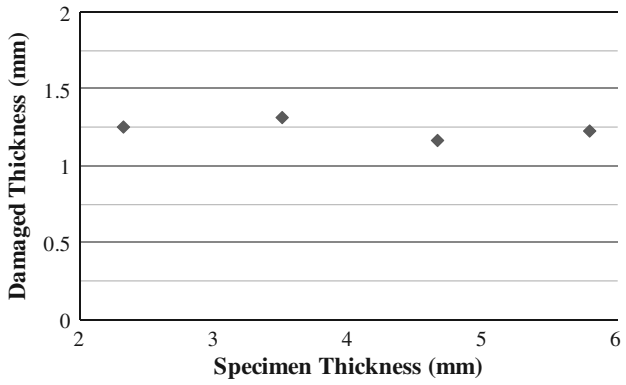

Fig. 15. Maximum damaged thickness variation for various specimen thicknesses (condition IV: 4/20 μs, 40 kA, t = 4.7 mm).

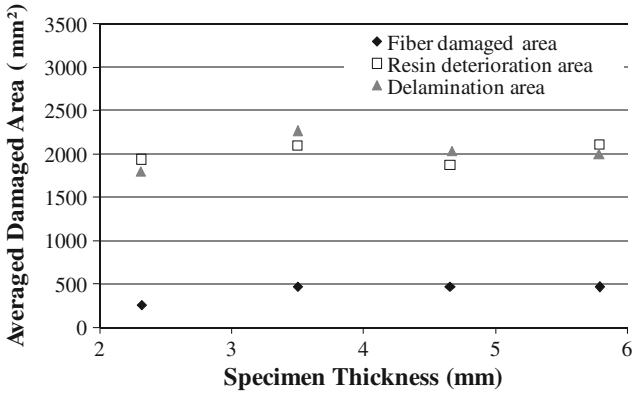

Fig. 16. Relationship between damaged area and specimen thickness (condition IV: 4/20 μs, 40 kA, t = 4.7 mm)

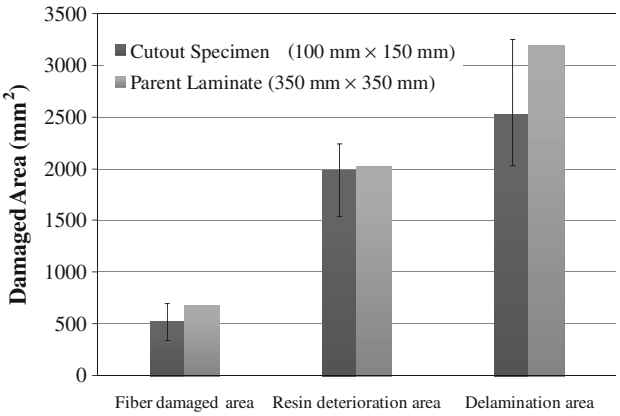

Fig. 17. Comparison of damage size between small specimens and parent laminate (condition IV: 4/20 μs, 40 kA).

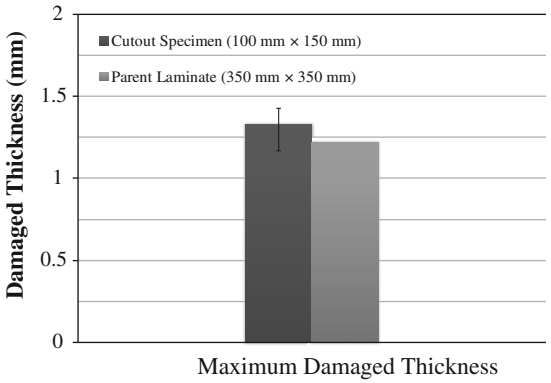

Fig. 18. Comparison of maximum damaged thickness between small specimens and parent laminate (condition IV: 4/20 μs, 40 kA).

damaged surface because of the strong orthotropic electrical properties of graphite/epoxy laminate. These strong orthotropic electrical properties generate a similar electrical current distribution in the thickness direction near the lightning attachment surface. As a result, varying the thickness of a specimen does not affect the size of damage in each damage mode.

An artificial lightning test on a large parent laminate was performed to understand the effect of specimen size variation on damage behavior. The size of the specimen used was 350 mm × 350 mm, stacking sequence was $[45/0/-45/90]_3$s, and averaged thickness was about 3.5 mm. An artificial lightning test was performed under condition IV (4/20 μs, 40 kA). The measured results for each damage mode due to a lightning strike are shown in Figs. 17 and 18. The ordinate is the measured delamination area. For comparison, the lightning test results for a cutout specimen (150 mm × 100 mm) are also shown in the figure. The results are averages of the results of the seven tests; the error bar represents the upper and lower bounds of the results for each damage mode in the seven tests.

The results show that, for all damage modes, there is no significant difference between the results of the parent laminate and those of cutout specimens; measured results for the parent laminate are within the error bar obtained from the cutout specimens. Although only one examination could be performed on the parent laminate because of limitations of the material, it is considered that the thickness and size of the specimens have little effect on damage size under the experimental conditions attempted in this study.

3.4. Waveform variation effect on damage size

Test results for various lightning parameter conditions using specimens of specific size and thickness are examined in detail to understand the effect of waveform and specific energy on the lightning damage behavior of graphite/epoxy laminated specimens. Since it has been determined in the previous section that size and thickness of a specimen have little effect on damage behavior,

Table 3
Coefficient of determinations R^2 of the regression result.

	Function type	Peak current	Electrical charge	Action integral
Fiber damaged area	Linear	**0.601**	0.518	0.24
Resin deterioration area	Linear	0.221	**0.932**	0.671
Damaged thickness	Linear	**0.263**	0.002	0.009
Delamination area	Exponential	0.002	0.676	**0.913**

the specimen of interest here is only 150 mm × 100 mm in size with a $[45/0/-45/90]_4$s stacking sequence. The lightning parameters of maximum current, waveform, electrical charge, and specific energy (action integral) are considered; the damage modes evaluated are the fiber damaged area, maximum damage depth, resin deterioration area, and delamination area. The most strongly correlated parameter against specific damage mode is examined by regression analysis with least square error method. Linear and exponential regression was examined to each damage mode. Then, the lightning parameter which shows the largest coefficient of determination R^2 is defined as the most strongly correlated parameter against the specific damage mode. The result of regression is shown in Table 3. The detailed description of regression analysis is shown in [17].

Each damage mode as measured following a lightning test is plotted using the most strongly correlated lightning parameter in Figs. 19–22.

The measured fiber damaged area shows the strongest correlation with the peak current (Fig. 19). Here, the abscissa is the peak current, and the ordinate is the measured fiber damaged area.

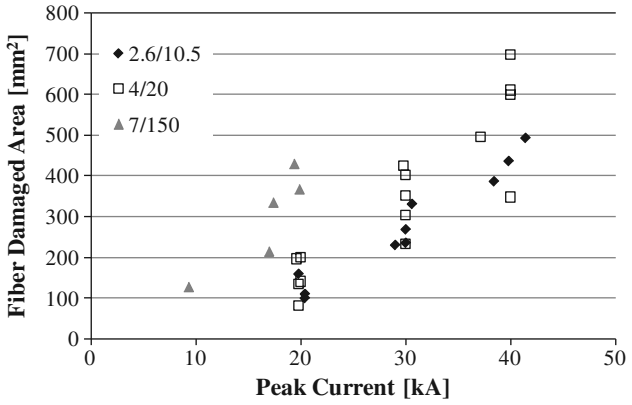

Fig. 19. Relationship between fiber damaged area and peak current.

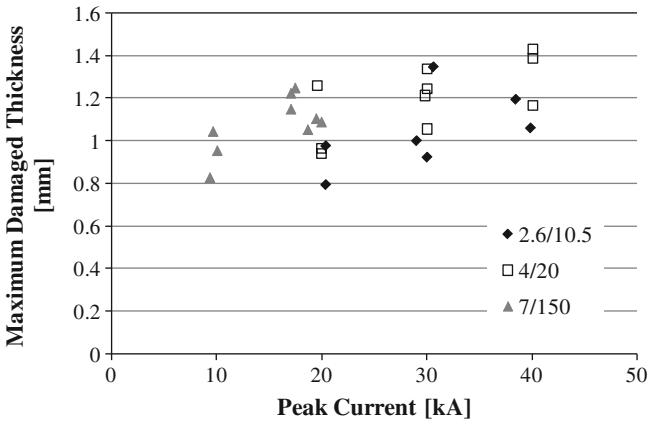

Fig. 20. Relationship between maximum damaged depth and peak current.

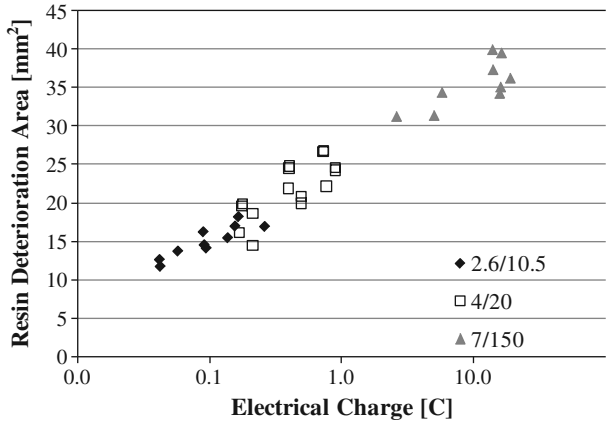

Fig. 21. Relationship between electrical charge and resin deterioration area.

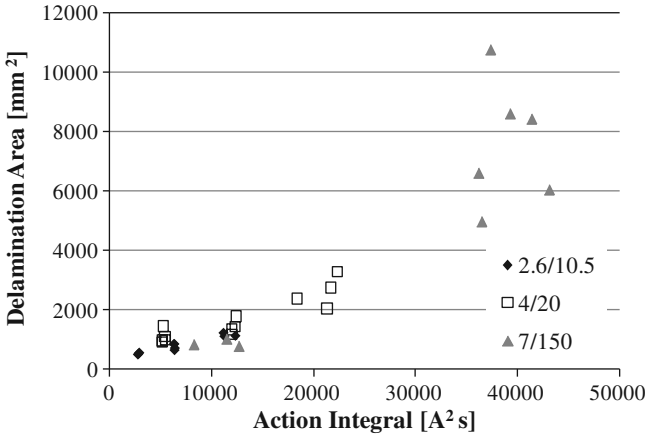

Fig. 22. Relationship between action integral and delamination area.

Although there is a variance, the measured fiber damaged area increases almost linearly with increased peak current. In particular, there are no significant differences between the results for the waveform of 2.6/10.5 μs and that of 4/20 μs, and the same size of fiber damaged area occurs with the same peak current. In the case of the 7/150 μs waveform applied using the ICG, a relatively large scatter was observed. As previously described, the modified IGV is functionally equivalent to the ICG. The measurement results of applied waveform with the modified IGV and the ICG shows the little difference between them (see Fig. 6a and b). However, considering the applied electrical energy (action integral), ICG applied 7–14 times larger electrical energy than the IGV applied in case of the identical peak current condition. It is considered that this large electrical energy makes difficult to apply stable discharge according to the target conditions with ICG, and this resulting in the large scatter.

The measured maximum damaged depths display the strongest correlation with the peak current (Fig. 20). The abscissa is the peak

current, and the ordinate is the measured maximum damaged depth. The maximum damaged depths were measured using the micro X-ray CT scanning system as in the previous section. Although there is a variance, the measured maximum damaged depth increases almost linearly with increasing peak current. As in the case of the fiber damaged area, it is considered that the effect of waveform variation on the maximum damaged depth is negligible.

The applied electrical charge (Eq. (1)) shows the strongest correlation with the measured resin deterioration area; Fig. 21 illustrates their relationship. The abscissa is the applied electrical charge, and the ordinate is the measured resin deterioration area. The measured resin deterioration area increases with increasing applied electrical charge. Here, the abscissa is shown as the logarithmic axis; the relationship between the applied electrical charge and the measured resin deterioration area is nonlinear. It is considered that the main cause of this resin deterioration is the combined effect of radiation heating due to high atmospheric temperature induced by insulation breakdown of air, and the resistive heating of specimen itself.

The results of the measured delamination area show a positive dependence on the applied specific energy (action integral) of the impulse current. In Fig. 22, the measured delamination area is plotted against the action integral of the applied impulse current. The action integral is defined in Eq. (2), and the product of the applied action integral and the electrical resistance of the target material is the generated Joule heat. This is the resistive heating due to the applied impulse current and the relatively high electrical resistance of the material, which results in the delamination of the CFRP laminate. Subsequent burning or pyrolysis of the resin around graphite fibers would result in delamination propagation inside the laminate. It is conjectured that the relatively large scatter of the results is due to the instability of the progress of damage caused by rapid evaporation of the resin.

As described above, it is shown that each damage mode produced by applying artificial lightning displays strong correspondence with a particular lightning parameter. The damage can be categorized into three modes: fiber damage mode, resin deterioration mode, and delamination mode. Since the damage in the thickness direction corresponds to the peak current as does the fiber damage mode, both damage modes can be assumed to be the same damage mode. When focusing on the waveform variation of applied artificial lightning, it is shown that the waveform has little effect on the damage response for each damage mode under the experimental conditions attempted in this study.

4. Conclusions

In this study, in order to investigate the damage behavior of graphite/epoxy laminate due to a lightning stroke and the relationship between lightning parameters and damage response, artificial lightning tests were performed using carefully selected experimental conditions. The following conclusions were obtained:

- The impulse current imitating natural lightning causes visible damage to the graphite/epoxy laminate. This damage can be categorized into three modes: fiber damage mode, resin deterioration mode, and delamination mode. Damage propagation in the in-plane direction in each layer is highly dependent on the orthotropic electrical properties of graphite/epoxy laminate.
- Each damage mode shows strong correlation with a particular lightning parameter; the fiber damaged area and damage thickness is governed by the peak current of the lightning stroke, while the resin deterioration area and the delamination projection area are determined by the electrical charge and the action integral of the waveform, respectively.

Variation of both specimen size and thickness has little effect on the damage response for each damage mode under the experimental conditions attempted in this study. Variation of the waveform of the applied impulse current also has an insignificant effect on the damage size and damage mode. In contrast, the damage size of each damage mode is highly dependent on the lightning parameters of the applied impulse current.

In this study, the specimens consist of the identical material and stacking sequence has been examined. However, it is essential to understand the influence of difference of materials and stacking sequence to the damage behavior against lightning strike. Therefore, further investigation regarding the factor affecting the lightning damage behavior of graphite/epoxy laminate is necessary for a greater understanding in our future work.

References

[1] Niu MCY. Composite airframe structures. Hong Kong: Conmilit Press Ltd.; 1993. p. 361–79.
[2] Ishikawa T, Sugimoto S, Matsushima M, Hayashi Y. Some experimental findings in CAI tests of CF/PEEK and conventional CF/EPOXY flat plates. Compos Sci Technol 1995;55:349–60.
[3] Ishikawa T, Aoki Y, Suemasu H. Pursuit of mechanical behavior in compression after impact (CAI) and open hole compression (OHC). In: Proceedings of ICCM-15, Durban, South Africa; 2005.
[4] Hitchen SA, Kemp RMJ. The effect of stacking sequence on impact damage in a carbon fibre/epoxy composite. Composites 1995;26(3):207–14.
[5] Richardson MOW, Wisheart MJ. Review of low-velocity impact properties of composite materials. Composites Part A 1996;27:1123–31.
[6] Stephenes CO. Advanced composite vertical stabilizer for DC-10 transport aircraft. NASA-CR-172780; 1979.
[7] Sandifer JP, Denny A, Wood MA. Fuel containment and damage tolerance in large composite primary aircraft structures. Phase 2: testing. NASA-CR-172519; 1985.
[8] Lightning direct effect handbook. AGATE-WP 3.1-031027-043; 2002.
[9] Baker A, Dutton S, Kelly D. Composite materials for aircraft structures. 2nd ed. Virginia: American Institute of Aeronautics and Astronautics Inc.; 2004. p. 461–2.
[10] Yokoyama S, Miyake K, Suzuki T, Kanao S. Winter lightning on Japan sea coast – development of measuring system on progressing feature of lightning discharge. IEEE Trans Power Delivery 1990;5:1418–25.
[11] Standard test method for compressive residual strength properties of damaged polymer matrix composite plates. ASTM D7137M-07, American Society for Testing and Materials (ASTM), West Conshohocken, PA, USA; 2007.
[12] Fisher FA, Plumer JA, Perala RA. Lightning protection of aircraft. NASA reference publication 1008; 1977.
[13] Aircraft lightning environment and related test waveforms standard. Committee report, AE4L-97-4; July 1997.
[14] Standard test method for measuring the damage resistance of a fiber-reinforced polymer matrix composite to a drop-weight impact event. ASTM D7136M-07, American Society for Testing and Materials (ASTM), West Conshohocken, PA, USA; 2007.
[15] Hirano Y, Todoroki A. Damage identification of woven graphite/epoxy composite beams using the electrical resistance change method. J Intell Mater Syst Struct 2007;18(3):253–63.
[16] Abry JC, Bochard S, Chateauminois A, Salvia M, Giraud G. In situ detection of damage in CFRP laminates by electrical resistance measurements. Compos Sci Technol 1999;59:925–35.
[17] Myers RH, Montgomery DC. Response surface methodology. 2nd ed. New York, USA: John Wiley & Sons, Inc.; 2002.